

LETTER TO THE EDITOR

# Discovery of benzyne, *o*-C<sub>6</sub>H<sub>4</sub>, in TMC-1 with the QUIJOTE<sup>1</sup> line survey<sup>★</sup>

J. Cernicharo<sup>1</sup>, M. Agúndez<sup>1</sup>, R. I. Kaiser<sup>2</sup>, C. Cabezas<sup>1</sup>, B. Tercero<sup>3,4</sup>, N. Marcelino<sup>1</sup>, J. R. Pardo<sup>1</sup>, P. de Vicente<sup>3</sup>

<sup>1</sup> Grupo de Astrofísica Molecular, Instituto de Física Fundamental (IFF-CSIC), C/ Serrano 121, 28006 Madrid, Spain  
e-mail: jose.cernicharo@csic.es

<sup>2</sup> Department of Chemistry, University of Hawaii at Manoa, Honolulu, HI 96822, USA

<sup>3</sup> Centro de Desarrollos Tecnológicos, Observatorio de Yebes (IGN), 19141 Yebes, Guadalajara, Spain

<sup>4</sup> Observatorio Astronómico Nacional (OAN, IGN), Madrid, Spain

Received; accepted

## ABSTRACT

We report the detection, for the first time in space, of a new non-functionalised hydrocarbon cycle in the direction of TMC-1: *o*-C<sub>6</sub>H<sub>4</sub> (ortho-benzyne). We derive a column density for this hydrocarbon cycle of  $(5.0 \pm 1.0) \times 10^{11}$  cm<sup>-2</sup>. The abundance of this species is around 30 times lower than that of cyclopentadiene and indene. We compare the abundance of benzyne with that of other pure hydrocarbons, cycles or chains, and find that it could be formed from neutral-radical reactions such as C<sub>2</sub>H + CH<sub>2</sub>CHCCH and C + C<sub>5</sub>H<sub>5</sub>, and possibly through C<sub>4</sub>H + C<sub>2</sub>H<sub>4</sub>, C<sub>3</sub>H + CH<sub>2</sub>CCH<sub>2</sub>, and C<sub>3</sub>H<sub>2</sub>+C<sub>3</sub>H<sub>3</sub>. Hence, the rich content of hydrocarbon cycles observed in TMC-1 could arise through a bottom-up scenario involving reactions of a few radicals with the abundant hydrocarbons recently revealed by the QUIJOTE line survey.

**Key words.** molecular data – line: identification – ISM: molecules – ISM: individual (TMC-1) – astrochemistry

## 1. Introduction

The recent discovery with the QUIJOTE<sup>1</sup> line survey of abundant hydrocarbons such as the propargyl radical (CH<sub>2</sub>CCH), vinylacetylene (CH<sub>2</sub>CHCCH), and ethynylallene (H<sub>2</sub>CCCHCCH) and cyclic hydrocarbons such as cyclopentadiene (*c*-C<sub>5</sub>H<sub>6</sub>) and indene (*c*-C<sub>9</sub>H<sub>8</sub>) in the cold dark cloud TMC-1 (Agúndez et al., 2021a; Cernicharo et al., 2021a,b,c; Burkhardt et al., 2021), as well as the detection of their cyano derivatives (McGuire et al., 2018, 2021) in the same source, points to a new and interesting chemistry that had been completely unforeseen by the most sophisticated state-of-the-art chemical models. The detection of indene, the first non-functionalised polycyclic aromatic hydrocarbons (PAHs) detected in space, in the unexpected environment of a cold starless core is surprising and introduces new challenges to our understanding of the place where these PAHs are formed in space.

Many efforts have been devoted over the last 40 years to understanding the chemical processes that lead to the formation of these molecular species (see e.g. Jones et al. 2011; Parker et al. 2012; Joblin & Cernicharo 2018). Circumstellar envelopes around carbon-rich asymptotic giant branch (AGB) stars have been suggested as the factories of PAHs (Cherchneff et al., 1992). However, PAHs are only detected in well-UV-illuminated regions of the interstellar medium. The detection of benzene in the carbon-rich protoplanetary nebula CRL 618 (Cer-

nicharo et al., 2001) suggests a bottom-up approach in which the small hydrocarbons that formed during the AGB phase, such as C<sub>2</sub>H<sub>2</sub> and C<sub>2</sub>H<sub>4</sub>, interact with the UV radiation produced by the star in its evolution to the white dwarf phase (Woods et al., 2002; Cernicharo, 2004). Other hypotheses involve the processing of dust grains around evolved stars, either through UV photons (Pilleri et al., 2015) or by chemical processes (Martínez et al., 2020). Hence, it has been surprising to see that pure PAHs and their cyanide derivatives have been found in TMC-1, which is well protected against UV radiation (Cernicharo et al., 2021c; Burkhardt et al., 2021; McGuire et al., 2018, 2021). It is unlikely that these molecules arise from a reservoir existing since the early stages of the cloud because these relatively small PAHs would not have survived the diffuse cloud stage. An in situ formation mechanism for benzene, cyclopentadiene, indene, and naphthalene must involve abundant hydrocarbons containing from two to five carbon atoms (Kaiser & Hansen, 2021). Moreover, some of these species should allow an easy cyclisation in bimolecular reactions to efficiently form the first aromatic ring – benzene (*c*-C<sub>6</sub>H<sub>6</sub>), benzyne (*c*-C<sub>6</sub>H<sub>4</sub>), the phenyl radical (*c*-C<sub>6</sub>H<sub>5</sub>), or any other species – from which larger PAHs can grow (Jones et al., 2011; Parker et al., 2012; McCabe et al., 2020; Doddipatla et al., 2021). The propargyl radical and the closed-shell hydrocarbons methyl-, vinyl-, and ethynylallene have been detected in TMC-1 with high abundances (Agúndez et al., 2021a; Cernicharo et al., 2021b,c). Detecting all possible products of the reactions between these hydrocarbons and radicals is a mandatory step towards understanding the chemistry of PAHs in cold dark clouds.

The name benzyne refers to three isomeric species with molecular formula *c*-C<sub>6</sub>H<sub>4</sub>, which are six-membered rings with four hydrogen atoms. They can be considered as derivatives of

<sup>★</sup> Based on observations carried out with the Yebes 40m telescope (projects 19A003, 20A014, 20D023, and 21A011). The 40m radio telescope at Yebes Observatory is operated by the Spanish Geographic Institute (IGN; Ministerio de Transportes, Movilidad y Agenda Urbana).

<sup>1</sup> Q-band Ultrasensitive Inspection Journey to the Obscure TMC-1 Environment

benzene molecules due to the loss of two hydrogen atoms. The most stable isomer is 1,2-didehydrobenzene (ortho-benzyne), followed by 1,3-didehydrobenzene (meta-benzyne) and the 1,4-didehydrobenzene (para-benzyne), placed at 147 and 220 kJ mol<sup>-1</sup> from the ortho-benzyne, respectively (Olsen, 1971). The molecular structure of ortho-benzyne (hereinafter referred to as benzyne or as *o*-C<sub>6</sub>H<sub>4</sub>) is interesting because it contains a formal triple bond ('-yne') within a six-membered ring (see Fig. 1). This peculiar structure confers a high reactivity, and thus it is a reactive intermediate in organic chemistry that plays an important role in aromatic nucleophilic substitution reactions. In addition, it is a potential key species in the formation of PAHs and soot in pyrolysis experiments of organic molecules (Hirsch et al., 2018).

In this letter we report the discovery of the ortho isomer of benzyne, *o*-C<sub>6</sub>H<sub>4</sub>, and we discuss the relative abundances of pure hydrocarbons, chains and cycles, in the context of chemical models that include new radical-neutral reactions involving the abundant hydrocarbons recently found in TMC-1 (Agúndez et al., 2021a; Cernicharo et al., 2021a,b,c). We also discuss the evolution of these molecules when the volume density increases due to the gravitational collapse of the core to form protostars and their dusty planetary disks.

## 2. Observations

New receivers, built within the Nanocosmos project<sup>2</sup> and installed at the Yebes 40m radio telescope, were used for the observations of TMC-1 ( $\alpha_{J2000} = 4^{\text{h}}41^{\text{m}}41.9^{\text{s}}$  and  $\delta_{J2000} = +25^{\circ}41'27.0''$ ). A detailed description of the system is given by Tercero et al. (2021). The receiver consists of two cold high electron mobility transistor amplifiers that cover the 31.0-50.3 GHz band with horizontal and vertical polarisations. Receiver temperatures in the runs achieved in 2020 vary from 22 K at 32 GHz to 42 K at 50 GHz. Some power adaptation in the down-conversion chains have reduced the receiver temperatures in 2021 to 16 K at 32 GHz and 25 K at 50 GHz. The back ends are  $2 \times 8 \times 2.5$  GHz fast Fourier transform spectrometers with a spectral resolution of 38.15 kHz, providing the whole coverage of the Q band in both polarisations. All observations were performed in the frequency switching mode. The main beam efficiency varies from 0.6 at 32 GHz to 0.43 at 50 GHz. The intensity scale used in this work, antenna temperature ( $T_A^*$ ), was calibrated using two absorbers at different temperatures and the atmospheric transmission model ATM (Cernicharo, 1985; Pardo et al., 2001). Calibration uncertainties were adopted to be 10 %. All data were analysed using the GILDAS package<sup>3</sup>.

The QUIJOTE line survey was performed in several sessions between 2019 and 2021. Previous QUIJOTE results on the detection of C<sub>3</sub>N<sup>-</sup> and C<sub>5</sub>N<sup>-</sup> (Cernicharo et al., 2020a), HC<sub>5</sub>NH<sup>+</sup> (Marcelino et al., 2020), HC<sub>4</sub>NC (Cernicharo et al., 2020b), and HC<sub>3</sub>O<sup>+</sup> (Cernicharo et al., 2020c) were based on two observing runs performed in November 2019 and February 2020. Two different frequency coverages were achieved during these runs, 31.08-49.52 GHz and 31.98-50.42 GHz, in order to check that no spurious spectral ghosts are produced in the down-conversion chain. In these observations the frequency throw was 10 MHz.

Additional data were taken in October 2020, December 2020, and January-May 2021. In these observations the selected frequency coverage was 31.08-49.52 GHz, and the frequency throw for the frequency switching observations was 8 MHz.

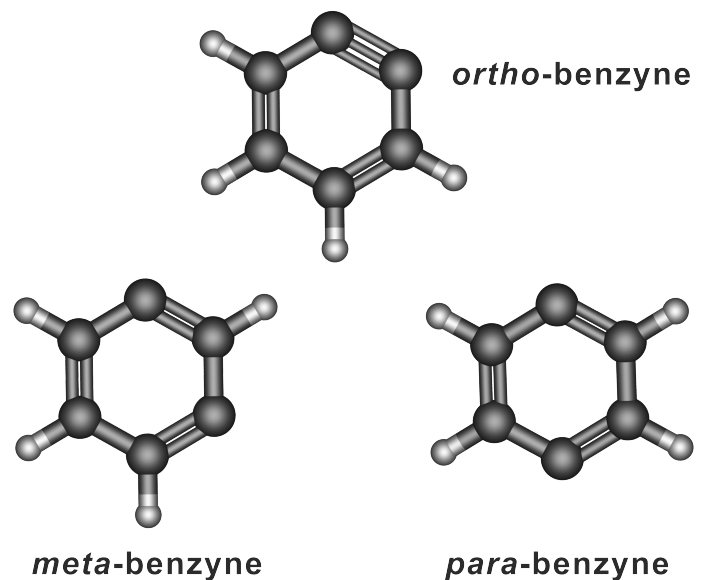


Fig. 1. Scheme of the ortho, para, and meta isomers of benzyne.

The two different frequency throws allow unambiguously negative features produced in the folding of the frequency switching data to be identified. These data allowed the detection of the acetyl cation, CH<sub>3</sub>CO<sup>+</sup> (Cernicharo et al., 2021d), HC<sub>3</sub>S<sup>+</sup> (Cernicharo et al., 2021e), the isomers of C<sub>4</sub>H<sub>3</sub>N (Marcelino et al., 2021), *l*-H<sub>2</sub>C<sub>5</sub> (Cabezas et al., 2021c), vinyl and allenyl acetylene (Cernicharo et al., 2021a,b), ethynyl cyclopropenylidene, cyclopentadiene, and indene (Cernicharo et al., 2021c). Several sulphur-bearing species (NCS, HCCS, H<sub>2</sub>CCS, H<sub>2</sub>CCCS, C<sub>4</sub>S, HCSCN, and HCSCCH) have also been detected with these data (Cernicharo et al., 2021f,g). In addition, some molecules typical of hot cores and corinos (C<sub>2</sub>H<sub>3</sub>CHO, C<sub>2</sub>H<sub>3</sub>OH, HCOOCH<sub>3</sub>, CH<sub>3</sub>OCH<sub>3</sub>, CH<sub>3</sub>CH<sub>2</sub>CN) and species typical of circumstellar envelopes (C<sub>5</sub>S, HCCN, HC<sub>4</sub>N) were also detected (Agúndez et al., 2021b; Cernicharo et al., 2021a). Last but not least, a significant number of singly and doubly deuterated species, such as HDCCN (Cabezas et al., 2021a), CH<sub>2</sub>DC<sub>3</sub>N (Cabezas et al., 2021b), and the D and <sup>13</sup>C doubly substituted isotopologues of HC<sub>3</sub>N (Tercero et al. 2021, in preparation), have also been observed for the first time in space thanks to QUIJOTE.

The total observing time on the source by May 2021 was 240 hours. QUIJOTE is a living line survey, and we expect a total observing time on the source of 450 hours by the end of 2021. The final goal of QUIJOTE, a sensitivity of 0.1 mK (lines of 0.5 mK detected at the 5 $\sigma$  level), will require around 1000 hours of observing time and will be reached by the winter of 2023-2024.

The sensitivity of our TMC-1 data is better than that of previously published line surveys of this source at the same frequencies (Kaifu et al., 2004) by a factor 20-30. Below 40 GHz the sensitivity is 0.2 mK, increasing slowly up to 0.5 mK at 49.5 GHz. Thanks to this achievement, it has been possible to detect many individual lines from molecules (Cernicharo et al., 2021a) that have been reported only by stacking techniques (Burkhardt et al., 2021). The level of sensitivity we have reached transforms TMC-1 into a source in which, although still far from the spectral confusion limit, the density of lines below 1 mK in intensity is particularly high. TMC-1 can no longer be considered as a line-poor source. Hence, the identification of new species requires a systematic exploration of the rotational transitions of single and double isotopologues of abundant species (see e.g. Cabezas et al. 2021a,b, Tercero et al. 2021, in preparation) before the detec-

<sup>2</sup> <https://nanocosmos.iff.csic.es/>

<sup>3</sup> <http://www.iram.fr/IRAMFR/GILDAS>

tion of a new species can be claimed. In this context, line identification in this work was done using the catalogues MADEX (Cernicharo, 2012), CDMS (Müller et al., 2005), JPL (Pickett et al., 1998), and Splatalogue<sup>4</sup>. By May 2021, the MADEX code contained 6369 spectral entries corresponding to the ground and vibrationally excited states, together with the corresponding isotopologues, of 1691 molecules.

### 3. Results

Our recent discovery of pure hydrocarbon cycles such as cyclopentadiene and indene (Cernicharo et al., 2021c) prompted us to search for other chemically related hydrocarbon cycles, benzyne (*o*-C<sub>6</sub>H<sub>4</sub>) being an obvious search candidate. The benzyne molecule is an asymmetric top with a *b* dipole directed along the C<sub>2v</sub> symmetry axis, estimated from ab initio calculations to be 1.38 D (Kraka & Cremer, 1993). Laboratory data for this species have been taken from Brown et al. (1986), Kukolich et al. (2003), and Robertson et al. 2003. The rotational levels of benzyne are subjected to spin statistics due to the presence of two pairs of equivalent hydrogen nuclei. As shown in Bunker & Jensen (1998), the nuclear statistical weight for the rotational levels with *K<sub>a</sub>* + *K<sub>c</sub>* even and odd is five and three, respectively (ortho and para species; these names refer to the symmetry states and are unrelated to the same names used to distinguish the different isomers). The first para level, 1<sub>0,1</sub>, is 0.42 K above the ground ortho state, 0<sub>00</sub>. Ortho-benzyne was previously searched for towards CRL618 without success (Widicus Weaver et al., 2007).

An examination of the QUIJOTE data quickly indicates that all ortho lines are detected with antenna temperatures between 0.5 and 1.8 mK. A total of seven ortho lines and four para lines are detected. Figure 2 shows the nine lines detected above 3 $\sigma$ . Two of the lines of para benzyne are detected only at the 3 $\sigma$  level and are not shown in this figure (see Table A.1). Nevertheless, their intensities are compatible with our model predictions. Table A.1 provides the line parameters of the observed lines. One of the para lines, the 3<sub>3,0</sub> – 2<sub>2,1</sub>, is fully blended with a line of 2 mK arising from D<sup>13</sup>CCCN (Tercero et al. 2021, in preparation). Three additional lines of the para species are below the 3 $\sigma$  detection limit at the corresponding frequencies (see Table A.1). Some interfering features produce partial blends with three lines of benzyne, as shown in Fig. 2. One of these features arises from a rotational transition of the *A* species of propylene and overlaps in frequency with the 7<sub>0,7</sub> – 6<sub>1,6</sub> transition of benzyne. From the derived column density of propylene by Marcelino et al. (2007), the expected contribution from the transition of benzyne is 0.5 mK. A couple of unidentified lines also have some partial blend with the 7<sub>0,7</sub> – 6<sub>1,6</sub> and 6<sub>1,5</sub> – 5<sub>2,4</sub> transitions of benzyne. However, the line parameters for these transitions can be derived reasonably well. All remaining lines in the Q band of benzyne are well below our present detection limit. At the present level of sensitivity of QUIJOTE, the number of unidentified lines becomes a concern when any stacking technique is used to detect molecules that produce weak emission. Our detection of benzyne based on the observation of several ortho and para lines is robust, reliable, and provides an accurate estimation of its column density.

An analysis of the observed intensities using a line profile fitting method (Cernicharo et al., 2021e) provides a rotational temperature of 7 $\pm$ 1 K and a total (ortho plus para) column density for benzyne of (5.0 $\pm$ 1.0) $\times$ 10<sup>11</sup> cm<sup>-2</sup>. In the fitting procedure we

considered the ortho and para levels as those of a single molecule with the corresponding statistical weights (5/3). A separate fit considering the two symmetry species separately and fixing the rotational temperature to 7 K provides similar results and an ortho/para ratio of 1.4 $\pm$ 0.6, which is consistent with the expected value of 5/3.

Adopting an H<sub>2</sub> column density of 10<sup>22</sup> cm<sup>-2</sup> for TMC-1 (Cernicharo & Guélin, 1987), the abundance of *o*-C<sub>6</sub>H<sub>4</sub> relative to H<sub>2</sub> is (5.0 $\pm$ 1) $\times$ 10<sup>-11</sup>. This is significantly below those of other cycles, such as *c*-C<sub>3</sub>H<sub>2</sub>, *c*-C<sub>3</sub>H<sub>6</sub>, and *c*-C<sub>9</sub>H<sub>8</sub> (Cernicharo et al., 2021a).

### 4. Chemistry

The detection of *o*-C<sub>6</sub>H<sub>4</sub> in TMC-1 raises interesting questions about its formation. The possible reactions leading to this molecule are discussed in Appendix B. To investigate the overall contribution of reactions (1) and (7) to the formation of *o*-C<sub>6</sub>H<sub>4</sub> in TMC-1, astrochemical models were exploited (see Fig. 3 and Appendix B). We built a pseudo-time-dependent gas-phase chemical model. We adopted typical parameters of cold dense clouds, namely a gas kinetic temperature of 10 K, a volume density of H<sub>2</sub> of 2 $\times$ 10<sup>4</sup> cm<sup>-3</sup>, a cosmic-ray ionisation rate of H<sub>2</sub> of 1.3 $\times$ 10<sup>-17</sup> s<sup>-1</sup>, a visual extinction of 30 mag, and the set of so-called ‘low-metal’ elemental abundances (see e.g. Agúndez & Wakelam 2013). We note that the volume density of H<sub>2</sub> in TMC-1 could be somewhat higher than that in our adopted value. The main effect of a slight increase in the density is that the abundance curves shift to shorter times, while peak abundances may increase or decrease slightly. The gas-phase chemical network is based on the RATE12 network from the UMIST database (McElroy et al., 2013), with updates relevant for the chemistry of CH<sub>2</sub>CCH, CH<sub>2</sub>CHCCH, H<sub>2</sub>CCCHCCH, and *c*-C<sub>3</sub>H<sub>6</sub> (Agúndez et al., 2021a; Cernicharo et al., 2021a,b,c). Benzyne was included and assumed to be formed by reactions (1) and (7) and destroyed by reactions with C atoms and C<sup>+</sup> and H<sup>+</sup> ions. The peak fractional abundance of *o*-C<sub>6</sub>H<sub>4</sub> is 3 $\times$ 10<sup>-13</sup> relative to H<sub>2</sub> (see model A in Fig. 3), which is well below the observed value, (5 $\pm$ 1) $\times$ 10<sup>-11</sup>. This suggests that alternative reactions besides (1) and (7) may contribute to *o*-C<sub>6</sub>H<sub>4</sub>.

Among these reactions, (2), (4), (5), (8), (9), (11), and (12) are unlikely to form *o*-C<sub>6</sub>H<sub>4</sub> (Appendix B). Reactions (3) and (6) are difficult to implement since the radicals C<sub>5</sub>H<sub>3</sub> and C<sub>4</sub>H<sub>5</sub> are not included in the UMIST database. Adding ill-defined radical reactions would add more uncertainty to the output of the models. However, the remaining reactions, (13) and (14) and potentially (10), are plausible routes to *o*-C<sub>6</sub>H<sub>4</sub>. Moreover, these reactions involve reactants that are abundant in TMC-1 (Fossé et al., 2001; Cabezas et al., 2021a; Agúndez et al., 2021a). Including these three reactions results in a peak abundance for *o*-C<sub>6</sub>H<sub>4</sub> of 3 $\times$ 10<sup>-11</sup> relative to H<sub>2</sub> (model B in Fig. 3), which is in good agreement with the observed value, (5 $\pm$ 1) $\times$ 10<sup>-11</sup>. Therefore, reactions (13), (14), and (10) deserve to be studied experimentally and theoretically in the future to understand how this highly reactive cyclic and aromatic molecule, *o*-C<sub>6</sub>H<sub>4</sub>, can be formed in TMC-1. It should be noted that benzyne could also be formed through ionic routes. For example, the dissociative recombination of the *c*-C<sub>6</sub>H<sub>5</sub><sup>+</sup> ion with electrons could produce *o*-C<sub>6</sub>H<sub>4</sub>. The precursor ion, *c*-C<sub>6</sub>H<sub>5</sub><sup>+</sup>, could in turn be formed through different ion-neutral reactions, such as C<sub>4</sub>H<sub>3</sub><sup>+</sup> + C<sub>2</sub>H<sub>2</sub> (Anicich 1993; see also Woods et al. 2002) or C<sub>3</sub>H<sub>3</sub><sup>+</sup> + CH<sub>2</sub>CCH.

It would be interesting to investigate whether *o*-C<sub>6</sub>H<sub>4</sub> could be formed upon the dissociative recombination of C<sub>6</sub>H<sub>5</sub><sup>+</sup> or C<sub>6</sub> ions with more than five H atoms.

<sup>4</sup> <https://splatalogue.online/advanced1.php>

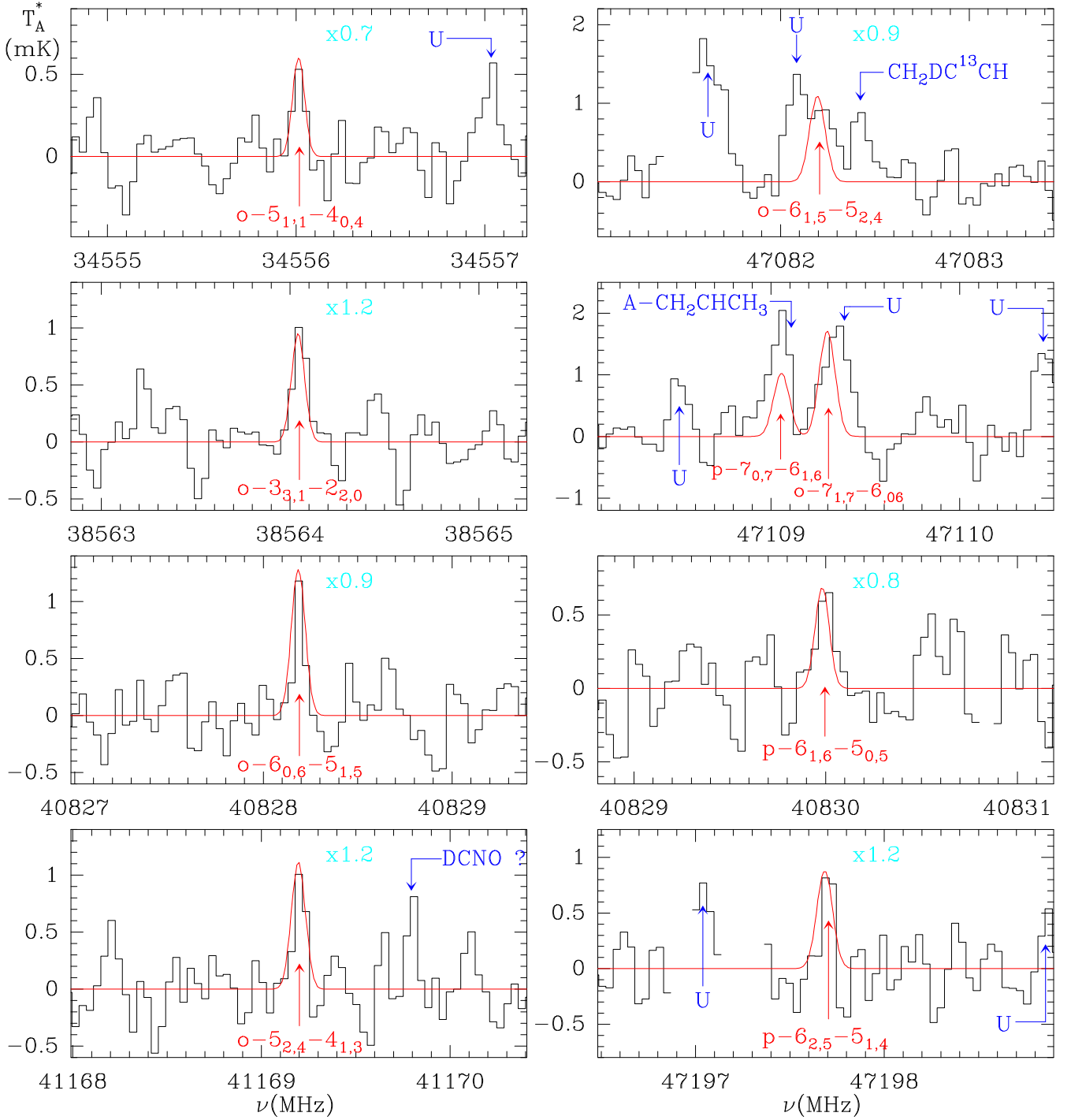


**Fig. 2.** Subset of the observed lines of  $o$ -C<sub>6</sub>H<sub>4</sub> in the 31–50 GHz frequency range towards TMC-1 (see Table A.1 for the complete list of detected benzyne lines). The abscissa corresponds to the rest frequency assuming a local standard of rest velocity of 5.83 km s<sup>-1</sup>. The ordinate is the antenna temperature corrected for atmospheric and telescope losses, in mK. The red line shows the synthetic spectrum obtained from a fit to the observed line profiles, which provides  $T_r = 7 \pm 1$  K and  $N(o\text{-C}_6\text{H}_4) = (5.0 \pm 1.0) \times 10^{11}$  cm<sup>-2</sup>. The rotational quantum numbers are indicated in each panel. Blanked channels correspond to negative features produced in the folding of the frequency switching data. Cyan numbers indicate the multiplicative factor applied to the best model, when needed, to match the observations.

## 5. Discussion and conclusions

The high abundance of hydrocarbon chains and cycles in TMC-1 suggests that one of the main sites of production of the seeds for PAH formation could be cold dark clouds and that this process could be a transitory one. Figure 3 shows that the peak of formation of  $o$ -C<sub>6</sub>H<sub>4</sub> and other hydrocarbons is produced in a few 10<sup>5</sup> years. When the density increases due to the collapse

of the cloud, most of these large hydrocarbons will stick onto dust grains. The chemistry of ices of cyclopentadiene, benzene, indene, and other species is poorly known as most experiments have been done with large PAHs. The dust grains enriched in these molecules, together with their pristine carbon composition produced during their early formation, will evolve with time and will become the constituents of the solid blocks that produce asteroids and planetesimals during the first stages of star and planet

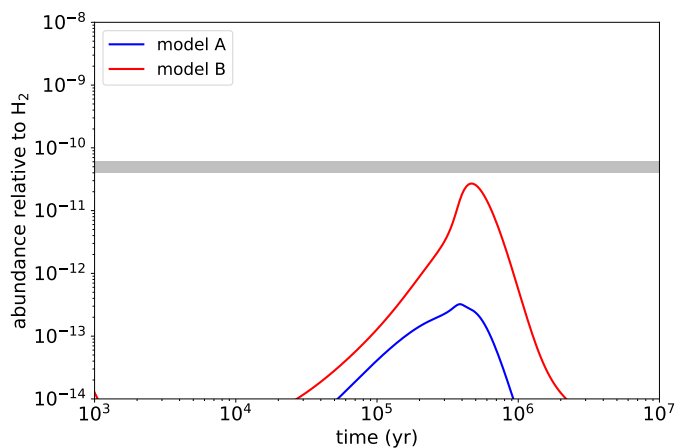


**Fig. 3.** Calculated fractional abundance of *o*-C<sub>6</sub>H<sub>4</sub> as a function of time in models A and B (see text). The horizontal grey band corresponds to the observed abundance in TMC-1.

formation. Eventually, some of these grains will be exposed to UV radiation from external and/or internal sources producing photodissociation regions. A significant fraction of the PAH emission observed in these regions could be due to PAHs formed from hydrocarbon-rich ices (Abplanalp et al., 2018; Kaiser & Roessler, 1997), and ices of cyclopentadiene, benzene, and indene deposited in a transitory phase of between 10<sup>5</sup> and 10<sup>6</sup> yr during the evolution of the cloud (we note that chemical times depend on the volume density and adopted initial physical and chemical conditions). None of these species have been found in the deep Q-band line survey of IRC +10216 performed with the Yebes 40m radio telescope (Pardo et al., 2021). While in the external layers of this carbon-rich circumstellar envelope the abundance of radicals is very high (Agúndez et al., 2017), the chemical time corresponding to these regions is relatively short, ~10<sup>4</sup> yr, implying that the first cycles may not have had enough time to be formed. A different context is that of carbon-rich protoplanetary nebulae such as CRL 618, where photodissociation and ionisation is enhanced with respect to the AGB phase and where benzene has been found from infrared observations with the Infrared Space Observatory (Cernicharo et al., 2001). Further, distinct temperature ranges from 10 K to a few thousand K facilitate diverse low- and high-temperature molecular mass growth processes (Cernicharo, 2004; Kaiser & Hansen, 2021).

To summarise, we report in this work the detection of the ortho isomer of benzyne, *o*-C<sub>6</sub>H<sub>4</sub>, in TMC-1. The observed abundance,  $(5\pm 1)\times 10^{-11}$  relative to H<sub>2</sub>, can be nicely reproduced with fractional abundances of  $3\times 10^{-11}$  considering that *o*-C<sub>6</sub>H<sub>4</sub> is formed by the neutral-neutral reactions C<sub>2</sub>H + CH<sub>2</sub>CHCCH and C + C<sub>5</sub>H<sub>5</sub> and possibly through the reactions C<sub>4</sub>H + C<sub>2</sub>H<sub>4</sub>, C<sub>3</sub>H + CH<sub>2</sub>CCH<sub>2</sub>, and C<sub>3</sub>H<sub>2</sub> + C<sub>3</sub>H<sub>3</sub>. With a sensitive line survey such as QUIJOTE, the discovery of new molecules can be performed in the classical line by line detection method. Hence, QUIJOTE provides unambiguous detection of new molecular species and reliable column density determinations.

**Acknowledgements.** We thank ERC for funding through grant ERC-2013-SyG-610256-NANOCOSMOS. M.A. thanks MICIU for grant RyC-2014-16277. We also thank Ministerio de Ciencia e Innovación of Spain (MICIU) for funding support through projects AYA2016-75066-C2-1-P, PID2019-106110GB-I00, PID2019-107115GB-C21 / AEI / 10.13039/501100011033, and PID2019-106235GB-I00.

## References

- Abplanalp, M.J., Jones, B.M., Kaiser, R.I. 2018, PCCP, 20, 5435  
 Agúndez, M. & Wakelam, V. 2013, Chem. Rev. 113, 8710  
 Agúndez, M., Cernicharo, J., Quintana-Lacaci, G., et al. 2017, A&A, 601, A4  
 Agúndez, M., Cabezas, C., Tercero, B., et al. 2021a, A&A, 647, L10  
 Agúndez, M., Marcelino, N., Tercero, B., et al. 2021b, A&A, 649, L4  
 Amich, V.G. 1993, J. Phys. Chem. Ref. Data, 22, 1469  
 Bertoloite, C., Le Picard, S. D., Balucani, N., et al. 2010, PCCP, 12, 3677  
 Bunker, P.R. & Jensen, P. 1998, Molecular Symmetry and Spectroscopy, 2nd edn. (Ottawa: NRC Research Press)  
 Burkhardt, A.M., Lee, L.K., Bryan Changala, P., et al. 2021, ApJ, 913, L18  
 Brown, R.D., Godfrey, P.D. & Rodler, M. 1986, J. Am. Chem. Soc. 108, 1296  
 Cabezas, C., Endo, Y., Roueff, E., et al. 2021a, A&A, 646, L1  
 Cabezas, C., Roueff, E., Tercero, B., et al. 2021b, A&A, 650, L15  
 Cabezas, C., Tercero, B., Agúndez, M., et al. 2021c, A&A, 650, L9  
 Canosa, A., Sims, I. R., Travers, D., et al. 1997, A&A, 323, 644  
 Cernicharo, J. 1985, Internal IRAM report (Granada: IRAM)  
 Cernicharo, J. & Guélin, M. 1987, A&A, 176, 299  
 Cernicharo, J., Heras, A.M., Tielens, A.G.G.M., et al. 2001, ApJ, 546, L123  
 Cernicharo, J. 2004, ApJ, 608, L41  
 Cernicharo, J., 2012, in ECLA 2011: Proc. of the European Conference on Laboratory Astrophysics, EAS Publications Series, 2012, Ed.: C. Stehl, C. Joblin, & L. d'Hendecourt (Cambridge: Cambridge Univ. Press), 251; [https://nanocosmos.iff.csic.es/?page\\_id=1619](https://nanocosmos.iff.csic.es/?page_id=1619)  
 Cernicharo, J., Marcelino, N., Pardo, J.R., et al. 2020a, A&A, 641, L9  
 Cernicharo, J., Marcelino, N., Agúndez, et al. 2020b, A&A, 642, L8  
 Cernicharo, J., Marcelino, N., Agúndez, M., et al. 2020c, A&A, 642, L17  
 Cernicharo, J., Agúndez, M., Cabezas, C., et al. 2021a, A&A, 647, L2  
 Cernicharo, J., Cabezas, C., Agúndez, M., et al. 2021b, A&A, 647, L3  
 Cernicharo, J., Agúndez, M., Cabezas, C., et al. 2021c, A&A, 649, L15  
 Cernicharo, J., Cabezas, C., Baillieux, S., et al. 2021d, A&A, 646, L7  
 Cernicharo, J., Cabezas, C., Endo, Y., et al. 2021e, A&A, 646, L3  
 Cernicharo, J., Cabezas, C., Agúndez, M., et al. 2021f, A&A, 648, L3  
 Cernicharo, J., Cabezas, C., Agúndez, M., et al. 2021g, A&A, 650, L14  
 Chastaigne, D., James, P. L., Sims, I. R., & Smith, I. W. M. 1998, Faraday Discussions, 109, 165  
 Cherchneff, I., Barker, J. R., & Tielens, A. G. G. M. 1992, ApJ, 401, 269  
 Kraka, E. & Cremer, D. 1993, Chem. Phys. Lett., 216, 333  
 Doddipatla, S., Galimova, G.R., Wei, H., et al. 2021, Science Advances, 7, eabd4044  
 Fossé, D., Cernicharo, J., Gerin, M., Cox, P. 2001, ApJ, 552, 168  
 Hahndorf, I., Lee, Y.T., Mebel, A.M. 2000, J. Chem. Phys., 113, 9622  
 Hahndorf, I., Lee, Y.T., Kaiser, R.I., et al. 2002, J. Chem. Phys., 116, 3248  
 Hirsch, F., Reusch, E., Constantinidis, P., et al. 2018, J. Phys. Chem. A, 122, 9563  
 Joblin, C. & Cernicharo, J. 2018, Science, 359, 156  
 Jones, B.M., Zhang, F., Kaiser, R.I., et al. 2011, PNAS, 108, 452  
 Kaifu, N., Ohishi, M., Kawaguchi, K., et al. 2004, PASJ, 56, 69  
 Kaiser, R.I. & Roessler, K. 1997, ApJ, 475, 144  
 Kaiser, R.I. 2002, Chem. Rev., 102, 1309  
 Kaiser, R.I., Gu, X., Zhang, F., & Maksyutenko, P., 2012, PCCP, 14, 575  
 Kaiser, R.I. & Hansen, N. 2021, J. Phys. Chem. A, 125, 3826  
 Kukulich, S.G., Tanjaroan, C., McCarthy, M.C. & Thaddeus, P. 2003, J. Chem. Phys., 119, 4353  
 Lide Jr, D.R. & Mann, D.E., 1957, J. Chem. Phys., 27, 868  
 McCabe, M.N., Hemberger, P., Reusch, E., et al. 2020, J. Phys. Chem. Lett., 11, 2859  
 McElroy, D., Walsh, C., Markwick, A. J., et al. 2013, A&A, 550, A36  
 McGuire, B.A., Burkhardt, A.M., Kalenskii, S., et al. 2018, Science, 359, 202  
 McGuire, B.A., Loomis, R.A., Burkhardt, A.M., et al. 2021, Science, 371, 1265  
 Marcelino, N., Cernicharo, J., & Agúndez, M. 2007, ApJ, 665, L127  
 Marcelino, N., Agúndez, M., Tercero, B., et al. 2020, A&A, 643, L6  
 Marcelino, N., Tercero, B., Agúndez, M., & Cernicharo, J. 2021, A&A, 646, L9  
 Martínez, L., Santoro, G., Merino, P., et al. 2020, Nature Astron., 4, 97  
 Mebel, A.M. & Kaiser, R.I. 2015, Int. Rev. Phys. Chem., 17, 21564  
 Müller, H.S.P., Schlöder, F., Stutzki, J., Winnewisser, G. 2005, J. Mol. Struct., 742, 215  
 Olsen, J.F. 1971, J. Mol. Struct., 8, 307  
 Parker, D.S.N., Zhang, F., Kim, Y.S., et al. 2012, PNAS, 109, 53  
 Pardo, J. R., Cernicharo, J., Serabyn, E. 2001, IEEE Trans. Antennas and Propagation, 49, 12  
 Pardo, J. R., et al. 2021, A&A, submitted  
 Pickett, H.M., Poynter, R. L., Cohen, E. A., et al. 1998, J. Quant. Spectrosc. Radiat. Transfer, 60, 883  
 Pilleri, P., Joblin, C., Boulanger, F. & Onaka, T. 2015, A&A, 577, A16  
 Robertson, E.G., Godfrey, P.D. & McNaughton, D. 2003, J. Mol. Spectrosc., 217, 123  
 Tercero, F., López-Pérez, J. A., Gallego, et al. 2021, A&A, 645, A37  
 Widicus Wwaver, S., Remijan, A.J., McMahon, R.J., and McCall, B.J. 2007, ApJ, L153  
 Woods, P.M., Millar, T. J., & Zijlstra, A.A. 2002, ApJ, 574, L167  
 Zhang, F., Parker, D., Kim, Y. S., et al. 2011, ApJ, 728, 141

## Appendix A: Benzynes line parameters

Line parameters were derived from a Gaussian fit to the observed lines using the GILDAS package. A velocity coverage of  $\pm 15 \text{ km s}^{-1}$  was selected for each line. Observed frequencies were derived assuming a local standard of rest velocity of  $5.83 \text{ km s}^{-1}$  (Cernicharo et al., 2020b). Observed velocities for the detected lines were determined assuming that rest frequencies are those predicted from the rotational and distortion constants provided by the fit to the laboratory data (Brown et al., 1986; Kukulich et al., 2003; Robertson et al., 2003). The predicted frequencies in MADEX (Cernicharo, 2012) agree within 1-5 kHz with those of the CDMS (Müller et al., 2005). Differences between predicted and observed frequencies never exceed  $1.5\sigma_{\Delta\nu}$ , where  $\Delta\nu$  is the estimated frequency uncertainty of the observed lines. The averaged  $V_{LSR}$  from the 11 observed lines of benzyne is  $5.80 \pm 0.05 \text{ km s}^{-1}$ , a value similar to that derived from all lines of  $\text{HC}_5\text{N}$  and its isotopologues in the Q band (Cernicharo et al., 2020b).

## Appendix B: The chemical network for the formation of benzyne

The low number densities of the reactants along with the typical 10 K translational temperature of a cold starless core such as TMC-1 only support barrierless and exoergic bimolecular reactions. Focusing on neutral-neutral reactions, the scheme is  $A + B \rightarrow [AB]^* \rightarrow C + D$ , where A and B represent the reactants,  $[AB]^*$  is the reaction intermediate(s), and C and D are the products (Kaiser, 2002). In TMC-1, the newly detected  $o\text{-C}_6\text{H}_4$  defines the product C; atomic hydrogen represents one of the most prominent counter fragments, D, that carry away a significant amount of the total angular momentum. This concludes that  $[AB]^*$  has to fulfil the stoichiometry of  $[\text{C}_6\text{H}_5]^*$ . Since the intermediate holds six carbon atoms, this can be achieved in bimolecular reactions in  $\text{C}_1\text{-C}_5$ ,  $\text{C}_2\text{-C}_4$ , and  $\text{C}_3\text{-C}_3$  systems with reactants at various degrees of hydrogenation. In principle, the following reactions, (1) to (14), could yield rovibrationally excited  $[\text{C}_6\text{H}_5]^*$  reaction intermediates, which undergo unimolecular decomposition via atomic hydrogen loss to form the newly detected  $o\text{-C}_6\text{H}_4$  molecule.

- (1)  $\text{C} + \text{C}_5\text{H}_5 \rightarrow o\text{-C}_6\text{H}_4 + \text{H}$
- (2)  $\text{CH} + \text{C}_5\text{H}_4 \rightarrow o\text{-C}_6\text{H}_4 + \text{H}$
- (3)  $\text{CH}_2 + \text{C}_5\text{H}_3 \rightarrow o\text{-C}_6\text{H}_4 + \text{H}$
- (4)  $\text{CH}_3 + \text{C}_5\text{H}_2 \rightarrow o\text{-C}_6\text{H}_4 + \text{H}$
- (5)  $\text{CH}_4 + \text{C}_5\text{H} \rightarrow o\text{-C}_6\text{H}_4 + \text{H}$
- (6)  $\text{C}_2 + \text{C}_4\text{H}_5 \rightarrow o\text{-C}_6\text{H}_4 + \text{H}$
- (7)  $\text{C}_2\text{H} + \text{C}_4\text{H}_4 \rightarrow o\text{-C}_6\text{H}_4 + \text{H}$
- (8)  $\text{C}_2\text{H}_2 + \text{C}_4\text{H}_3 \rightarrow o\text{-C}_6\text{H}_4 + \text{H}$
- (9)  $\text{C}_2\text{H}_3 + \text{C}_4\text{H}_2 \rightarrow o\text{-C}_6\text{H}_4 + \text{H}$
- (10)  $\text{C}_2\text{H}_4 + \text{C}_4\text{H} \rightarrow o\text{-C}_6\text{H}_4 + \text{H}$
- (11)  $\text{C}_2\text{H}_5 + \text{C}_4 \rightarrow o\text{-C}_6\text{H}_4 + \text{H}$
- (12)  $\text{C}_3 + \text{C}_3\text{H}_5 \rightarrow o\text{-C}_6\text{H}_4 + \text{H}$
- (13)  $\text{C}_3\text{H} + \text{C}_3\text{H}_4 \rightarrow o\text{-C}_6\text{H}_4 + \text{H}$
- (14)  $\text{C}_3\text{H}_2 + \text{C}_3\text{H}_3 \rightarrow o\text{-C}_6\text{H}_4 + \text{H}$ .

Among these reactions, only the reaction between the ethynyl radical ( $\text{C}_2\text{H}$ ) and vinylacetylene ( $\text{CH}_2\text{CHCCH}$ ), reaction (7), has been studied via crossed molecular beam experiments and electronic structure calculations (Zhang et al., 2011). This reaction is barrierless and exoergic, and thus it is expected to be fast at low temperatures. This finding is in line with the known high reactivity of  $\text{C}_2\text{H}$  radicals with unsaturated hydrocarbons at low temperatures (Chastaing et al., 1998), revealing rates of up to  $4 \times 10^{-10} \text{ cm}^3 \text{ s}^{-1}$ . Moreover, Zhang et al. (2011)

predicted that  $o\text{-C}_6\text{H}_4$  is formed with a branching ratio of up to 20% at 10 K, thus providing an effective rate of  $8 \times 10^{-11} \text{ cm}^3 \text{ s}^{-1}$ . Reaction (7) is thus a plausible route to benzyne in TMC-1. Further, in analogy to the  $\text{C}(\text{P})$ -benzene system (Hahndorf et al., 2002), the reaction of atomic carbon ( $\text{C}(\text{P})$ ) with cyclopropadienyl ( $c\text{-C}_3\text{H}_3$ ) – although studied neither experimentally nor computationally – is expected to form  $o\text{-C}_6\text{H}_4$  plus atomic hydrogen (reaction (1)). Hahndorf et al. (2000) predicted computationally that the propargyl radical ( $\text{C}_3\text{H}_3$ ) can react barrierlessly and exoergically with the vinyl radical ( $\text{C}_2\text{H}_3$ ) on the singlet surface to form  $c\text{-C}_5\text{H}_5$  plus atomic hydrogen, thus providing the  $c\text{-C}_5\text{H}_5$  required for reaction (1).

### Appendix B.1: Discounted reactions to benzyne

Reaction (2) has never been studied in the laboratory with any isomer such as methylacetylene ( $\text{HCCCCCH}_3$ ), penta-1,4-diyne ( $\text{CH}_2(\text{C}_2\text{H})_2$ ), or 1,2,3,4-pentatetraene ( $\text{H}_2\text{CCCCCH}_2$ ). Rate constant measurements of methylidyne ( $\text{CH}$ ) with unsaturated hydrocarbons by Canosa et al. (1997) reveal barrierless pathways with rates of a few  $10^{-10} \text{ cm}^3 \text{ s}^{-1}$ . However, crossed molecular beam reactions indicate that the  $\text{CH}$  radical adds to the double or triple bond of, for example, acetylene, ethylene, diacetylene, allene, and methylacetylene, followed by isomerisation through the ring opening and/or hydrogen shifts, followed by hydrogen atom losses. Six-membered ring formation only occurs through the ring expansion of an existing five-membered ring (i.e. a hypothetical cyclic  $c\text{-C}_5\text{H}_4$  isomer). However, no confirmed formation routes to cyclic  $c\text{-C}_5\text{H}_4$  are known so far; therefore, we do not include reaction (2) as a contributor to benzyne.

Reaction (4), which has never been studied either computationally nor experimentally, involves the addition of a methyl radical ( $\text{CH}_3$ ) to a triplet carbene ( $\text{HCCCCCH}$ ). The addition of a methyl radical to triple bonds of the ethynyl moiety involves barriers of up to  $50 \text{ kJ mol}^{-1}$ , which cannot be overcome in TMC-1. Methyl radicals could add barrierlessly to the central carbon atom, which essentially carries the unpaired electrons. However, this requires small, nearly zero-impact parameters and an extensive reorganisation of the carbon skeleton; therefore, although exoergic by  $207 \text{ kJ mol}^{-1}$  overall, the formation of benzyne is unlikely.

Reaction (5) represents a direct reaction that leads, via hydrogen abstraction, to a methyl radical plus  $\text{C}_5\text{H}_2$  molecules; although never studied experimentally, this hydrogen abstraction is expected to have a barrier. Further, this reaction is endoergic by  $27 \text{ kJ mol}^{-1}$  and hence cannot take place at 10 K. Reaction (5) cannot form  $o\text{-C}_6\text{H}_4 + \text{H}$  at 10 K since hydrogen abstraction represents the only feasible pathway.

Reaction (8) has an entrance barrier of addition of the  $\text{C}_4\text{H}_3$  with its radical centre to the carbon-carbon triple bond of acetylene  $25\text{--}37 \text{ kJ mol}^{-1}$ . Hence, its reaction is closed at 10 K as well.

Reaction (9) involves the reaction of a vinyl radical with diacetylene; reactions of vinyl radicals with closed-shell olefins and alkynes have entrance barriers of 10 to  $35 \text{ kJ mol}^{-1}$ , which cannot be overcome in TMC-1. This has been confirmed computationally (Zhang et al. 2011). Finally, reaction (11) and, in particular, reaction (12) likely have entrance barriers (Mebel & Kaiser, 2015).

**Table A.1.** Observed line parameters of benzyne.

Transition	$\nu_{pred}^a$ (MHz)	$\nu_{obs}^b$ (MHz)	$\int T_A^* dv^c$ (mK km s <sup>-1</sup> )	$\nu_{LSR}^d$ (km s <sup>-1</sup> )	$\Delta\nu^e$ (km s <sup>-1</sup> )	$T_A^{*f}$ (mK)	N
ortho state							
4 <sub>1,3</sub> – 3 <sub>2,2</sub>	33482.756(1)	33482.786(30)	0.34(07)	5.56(07)	0.66(18)	0.48(17)	
5 <sub>1,5</sub> – 4 <sub>0,4</sub>	34556.013(2)	35556.013(30)	0.36(10)	5.83(09)	0.63(18)	0.55(18)	
3 <sub>3,1</sub> – 2 <sub>2,0</sub>	38564.042(1)	38564.054(30)	0.74(15)	5.74(07)	0.68(17)	1.02(20)	
6 <sub>0,6</sub> – 5 <sub>1,5</sub>	40828.169(4)	40828.169(20)	0.54(11)	5.83(05)	0.45(10)	1.19(22)	
5 <sub>2,4</sub> – 4 <sub>1,3</sub>	41169.208(2)	41169.205(20)	0.56(13)	5.85(07)	0.48(12)	1.09(24)	
6 <sub>1,5</sub> – 5 <sub>2,4</sub>	47082.207(4)	47082.207(30)	0.87(30)	5.83(16)	0.87(30)	0.94(27)	
7 <sub>1,7</sub> – 6 <sub>0,6</sub>	47109.298(7)	47109.345(30)	1.91(25)	5.53(10)	1.02(15)	1.77(35)	A
para state							
5 <sub>0,5</sub> – 4 <sub>1,4</sub>	34543.093(2)					≤0.70	
4 <sub>2,3</sub> – 3 <sub>1,2</sub>	35656.830(1)					≤0.75	
5 <sub>1,4</sub> – 4 <sub>2,3</sub>	40595.926(2)	40595.919(30)	0.16(08)	5.90(12)	0.40(15)	0.47(17)	
6 <sub>1,6</sub> – 5 <sub>0,5</sub>	40829.994(4)	40830.000(30)	0.55(19)	5.79(13)	0.78(39)	0.67(27)	
3 <sub>3,0</sub> – 2 <sub>2,1</sub>	41071.944(1)						B
4 <sub>3,2</sub> – 3 <sub>2,1</sub>	45028.539(1)					≤0.75	
7 <sub>0,7</sub> – 6 <sub>1,6</sub>	47109.056(7)	47109.044(20)	1.63(21)	5.90(08)	0.80(13)	1.92(27)	C
6 <sub>2,5</sub> – 5 <sub>1,4</sub>	47197.685(4)	47197.708(30)	0.45(11)	5.72(20)	0.45(15)	0.95(26)	

**Notes.**

Values between parentheses correspond to the uncertainties of the parameters in units of the last significant digits.

Upper limits correspond to  $3\sigma$  values.

<sup>(a)</sup> Predicted frequency from the rotational and distortion constants derived from a fit to the lines observed by Brown et al. (1986), Kukolich et al. (2003), and Robertson et al. (2003).

<sup>(b)</sup> Observed frequency assuming a  $\nu_{LSR}$  of 5.83 km s<sup>-1</sup>.

<sup>(c)</sup> Integrated line intensity in mK km s<sup>-1</sup>.

<sup>(d)</sup>  $\nu_{LSR}$  assuming that the predicted frequencies are the rest frequencies of the lines (in km s<sup>-1</sup>).

<sup>(e)</sup> Line width at half intensity derived by fitting a Gaussian function to the observed line profile (in km s<sup>-1</sup>).

<sup>(f)</sup> Antenna temperature in millikelvin.

<sup>(A)</sup> Possibly a blend with a U line at +35 kHz of the predicted frequency.

<sup>(B)</sup> Blended with a line of D<sup>13</sup>CCCN. Fit unreliable.

<sup>(C)</sup> Blended with a line of CH<sub>2</sub>CHCH<sub>3</sub> with an expected intensity of 0.5 mK.